

International Journal of Modern Physics E
 © World Scientific Publishing Company

Probing the density dependence of symmetry energy at subsaturation density with HICs

Yingxun Zhang, M.B.Tsang, Zhuxia Li, P. Danielewicz, W.G. Lynch, Xiaohua Lu

*Department of Nuclear Physics, China Institute of Atomic Energy,
 Beijing, 102413, China*

*JINA/NSCL, Michigan State University,
 East Lansing, MI, 48824, USA*

The reaction mechanism of the central collisions and peripheral collisions for $^{112,124}\text{Sn} + ^{112,124}\text{Sn}$ at $E/A = 50\text{MeV}$ is investigated within the framework of the Improved Quantum Molecular Dynamics model. The results show that multifragmentation process is an important mechanism at this energy region, and the influence of the cluster emission on the double n/p ratios and the isospin transport ratio are important. Furthermore, three observables, double n/p ratios, isospin diffusion and the rapidity distribution of the ratio R_7 for $^{112,124}\text{Sn} + ^{112,124}\text{Sn}$ at $E/A=50\text{MeV}$ are analyzed with the Improved Quantum Molecular Dynamics model. The results show that these three observables are sensitive to the density dependence of the symmetry energy. By comparing the calculation results to the data, the consistent constraint on the density dependence of the symmetry energy from these three observables is obtained.

1. Introduction

The Equation of State (EOS) of asymmetric nuclear matter can be written approximately as $E(\rho, \delta) = E(\rho, \delta = 0) + E_{sym}(\rho)\delta^2 + \mathcal{O}(\delta^4)$, with $\delta = (\rho_n - \rho_p)/(\rho_n + \rho_p)$. It closely relates to different areas of nuclear physics, such as the nuclear structure of finite nuclei, dynamics process of neutron rich heavy ion collisions, physics of neutron star, et.al.^{1,2,3,4,5,6,7}. For the symmetry nuclear matter, measurements of isoscalar collective vibrations, collective flow and kaon production in energetic nucleus-nucleus collisions have constrained the EOS from normal density to five times saturation density^{8,9,10}. However, large uncertainties exist on the theoretical prediction on the density dependence of the EOS for neutron matter¹¹. So, determining the density dependence of the symmetry energy, $E_{sym}(\rho)$, becomes one of the main goals in nuclear physics at present and in the near future and has stimulated many theoretical and experimental studies. Heavy ion collisions with neutron-rich nuclei provide a unique opportunity to obtain the information of the density dependence of the symmetry energy in the laboratories because large extent of density can be formed during the HICs. Many useful observables from HICs, such as isoscaling of the isotope^{12,13,14}, isospin diffusion^{15,16,17,18}, neutron to proton yield ratios and its flow at intermediate heavy ion collisions have been proposed

2 *Yingxun Zhang*

and studied both theoretically and experimentally in order to constrain the density dependence of symmetry energy at subsaturation density. And π^-/π^+ ratios and its flow in high energy HICs was proposed to constrain the density dependence of the symmetry energy at supersaturation density^{19,20,21,22,23,24,25,26}.

Since the complex cluster production are observed in experiment for intermediate energy HICs, it is necessary to investigate the effects of clusters emission on these observables, neutron to proton ratios and isospin diffusion. As a microscopic dynamical n-body transport theory, formation of fragments is included automatically in the QMD type model. So, the ImQMD05^{19,27,28,34} model is suitable to study the impacts of the cluster formation on the isospin sensitive observables, such as n/p ratios for emitted nucleons and isospin diffusion for central collision and peripheral collisions at $E/A = 50\text{MeV}$ for $\text{Sn} + \text{Sn}$. Fig.1 shows the contour plots of multiplicity of fragments with charge Z as a function of its scaled rapidity $y/y_{beam}^{c.m.}$ at $E/A = 50\text{MeV}$ calculated with soft symmetry energy ($\gamma_i = 0.5$) for different impact parameters, $b = 2, 6, 8\text{fm}$, respectively. In general, one can observe

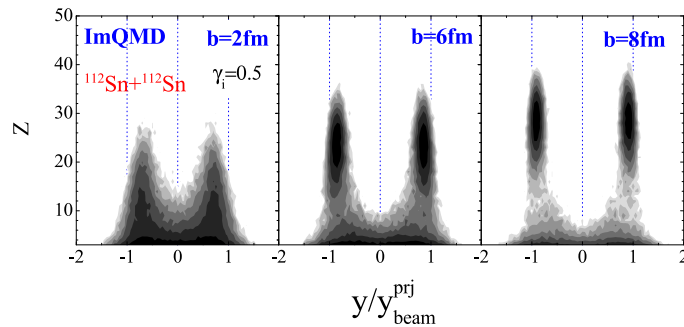


Fig. 1. The contour plots of multiplicity of fragments with charge Z as a function of its scaled rapidity $y/y_{beam}^{c.m.}$ for $^{112}\text{Sn} + ^{112}\text{Sn}$ at $E/A = 50\text{MeV}$ for $b = 2, 6, 8\text{fm}$ with $\gamma_i = 0.5$ cases.

two peaks on the rapidity distribution for the charge Z of fragments from central collisions to peripheral collisions, and the intermediate mass fragments can be formed from middle rapidity to projectile/target rapidity for central collisions and peripheral collisions. In detail, the maximum charge of fragments at mid-rapidity decrease from $Z \sim 15$ to $Z \sim 8$ with the impact parameter b increasing, and same for its yield. Furthermore, the heaviest fragments have lost about 35% of their initial velocity for central collisions and about 25% (10%) of their initial velocity for $b = 6\text{fm}$ ($b = 8\text{fm}$). The quantities of velocity loss for heaviest fragments depend on the decelerating effects from the effective n-n interactions and nucleon-nucleon collision in the participant region, and the multiplicity of fragments formed below the normal density in HICs. Through above discussion, one can see that the clusters formation plays an important role at intermediate energy HICs from central

to peripheral collisions and the effects of cluster emission on the isospin sensitive observables could not be ignored.

In order to study the density dependence of symmetry energy and the influence of cluster emission on the isospin sensitive observables, the density dependence of symmetry energy in nuclear matter:

$$E_{sym}(\rho) = \frac{1}{3} \frac{\hbar^2}{2m} \rho_0^{2/3} \left(\frac{3\pi^2}{2} \frac{\rho}{\rho_0} \right)^{2/3} + \frac{C_s}{2} \left(\frac{\rho}{\rho_0} \right)^{\gamma_i} \quad (1)$$

is introduced. C_s is the symmetry potential strength parameters, and γ_i give the density dependence of symmetry energy. The different density dependence of symmetry energy can be realized by varying γ_i in the ImQMD model.

2. The n/p ratios, isospin diffusion and the cluster emission effects

The neutron to proton ratio $R_{n/p} = \frac{dM_n(A)/dE_{cm}}{dM_p(A)/dE_{cm}}$ of pre-equilibrium emitted neutron over proton spectra was considered as a sensitive observable to the density dependence of symmetry energy²¹, because it has a straightforward link to the symmetry energy. In order to reduce the sensitivity to uncertainties in the neutron detection efficiencies and sensitivity to relative uncertainties in energy calibrations of neutrons and protons, the double ratio

$$DR(n/p) = R_{n/p}(A)/R_{n/p}(B) = \frac{dM_n(A)/dE_{cm}}{dM_p(A)/dE_{cm}} / \frac{dM_n(B)/dE_{cm}}{dM_p(B)/dE_{cm}} \quad (2)$$

had been measured by Famiano and compared with the transport model prediction^{20,21}.

We have performed calculations of collisions at an impact parameter of $b = 2fm$ at an incident energy of $50MeV$ per nucleon for two systems: $A = {}^{124}Sn + {}^{124}Sn$ and $B = {}^{112}Sn + {}^{112}Sn$ ¹⁹ with ImQMD05 to study the $DR(n/p)$ ratio for emitted nucleons. The shaded regions in the left panel of Fig.2 (a) show the range, determined by uncertainties in the simulations, of predicted double ratios $DR(n/p) = R_{n/p}(A)/R_{n/p}(B)$ of the nucleons emitted between 70° and 110° in the center of mass frame as a function of the center of mass nucleon energy, for $\gamma_i = 0.5$ and 2. The double ratios $DR(n/p)$ are higher for the EOS with the weaker symmetry energy density dependence $\gamma_i = 0.5$ than that for $\gamma_i = 2.0$ because the nucleons mainly emit from the lower density region at intermediate energy HICs. Compare to the data on $DR(n/p)$ for emitted nucleons (solid stars), the general trend of data $DR(n/p)$ are qualitatively reproduced and the data seem to be closer to the calculation employing the EOS with $\gamma_i = 0.5$. The fig.2 (b) show the coalescence-invariant double ratio. The coalescence-invariant double ratios are constructed by including all neutrons and protons emitted at a given velocity, regardless of whether they are emitted free or within a cluster. The data are shown as open stars and the calculation results are shown as shaded region in the right panel of figure 2(b). Here, the measurements and simulations results illustrate that the fragments with

4 *Yingxun Zhang*

$Z \geq 2$ mainly contribute to the low energy spectra and do not affect the high-energy $DR(n/p)$ data very much.

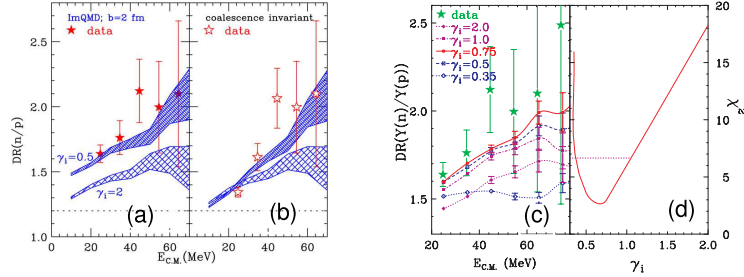


Fig. 2. (a) $DR(n/p)$ ratios for emitted free nucleons and (b) coalescent-invariant $DR(n/p)$ from the ImQMD simulations are plotted as shadow region. Data (star) from NSCL¹⁹. (c) $DR(n/p)$ ratios for different γ_i for central collisions, Data (star) from NSCL. (d) χ^2 analysis on the $DR(n/p)$ ratios³⁶.

In order to constrain the range of γ_i from the $DR(n/p)$ data that had been published, a series calculations for two systems, $A = {}^{124}\text{Sn} + {}^{124}\text{Sn}$ and $B = {}^{112}\text{Sn} + {}^{112}\text{Sn}$, have been performed by varying $\gamma_i = 0.35, 0.5, 0.75, 1.0$ and 2.0 (line with symbols)³⁶. As shown in fig.2(c), the computation uncertainties are statistical. It is known that emitted nucleons mainly from the subnormal densities at this energies. So, the n/p ratios of emitted nucleons are associated with the values of symmetry energy at subnormal density. Therefore, the $DR(n/p)$ ratio should increase with decreasing γ_i . However, in the limit of very small $\gamma_i \ll 0.35$, the system completely disintegrates and the $DR(n/p)$ ratio decrease and approaches the limit of reaction system, $(N/Z)_{124}/(N/Z)_{112} = 1.2$. As a consequence of these two competing effects, the double ratio values peak around the $\gamma_i = 0.7$. Despite the large experiment uncertainties for higher energy data, those comparisons definitely rule out very soft ($\gamma_i = 0.35$) and very stiff ($\gamma_i = 2.0$) density dependence of symmetry energy. Fig.2(d) shows the dependence on γ_i of the total χ^2 computed from the difference between predicted and measured double ratios. Within a 2σ uncertainty, parameters of γ_i fall in the range of $0.4 \leq \gamma_i \leq 1.05$ for the $C_s = 35.2\text{MeV}$.

It has been proved that the isospin diffusion ability depends on the strength of the symmetry energy in HICs^{15,16,35}. In order to quantify the isospin diffusion degree in heavy ion collisions, the isospin transport ratios R_i

$$R_i = (2X - X_{A+A} - X_{B+B}) / (X_{A+A} - X_{B+B}) \quad (3)$$

has been introduced¹⁵. The subscript A and B represent the neutron rich and neutron-poor nuclei, and the $A = {}^{124}\text{Sn}$, $B = {}^{112}\text{Sn}$ in this work. The value of R_i is obtained through 3 reaction systems at least, $A + A$, $B + B$ and $A + B$ (or $B + A$).

Where X is the isospin tracer from the isospin asymmetry nuclear reaction system $A + B$ (or $B + A$). The non-isospin diffusion effects are minimized by scaling the isospin observables with the same observables from the symmetric collisions of the neutron-rich $A + A$ and neutron-deficient $B + B$ systems using the isospin transport ratio defined as above. Adopting the Eq.3 definition on R_i , one can expect $R_i = \pm 1$ in absence of isospin diffusion. In the opposite, $R_i \approx 0$ if isospin equilibrium is achieved. Eq.3 also dictates that different observable, X , can give the same results if they are linearly related^{15,17}. In experiment, the X is taken as the isoscaling parameter $X_\alpha = \alpha$ and the yield ratios of $A = 7$ mirror nuclei, $X_7 = \ln(Y(^7Li)/Y(^7Be))$ for peripheral HICs^{15,17}. In order to analyze the isospin diffusion data with transport model, the observable $X = \delta$, the isospin asymmetry constructed from the fragments and free nucleons at the relevant rapidities is adopted in ImQMD. It has been confirmed theoretically and experimentally that there is a linear relationship between $X_{exp} = X_7, X_\alpha$ and $X_{th} = \delta$, and the relationship $R(X = \alpha) = R_7(X = X_7) = R(\delta)$ holds^{13,32,33,36}.

The left panel in Fig.3 show the ImQMD predictions on the $R(X = \delta)$ (lines) near the projectile rapidity as a function of impact parameters b for different $\gamma_i = 0.35, 0.5, 0.75, 1$ and 2^{36} . Faster equilibration occurs for smaller γ_i values which correspond to a larger symmetry energy at subnormal densities. Thus, we see a monotonic decrease of the absolute values of $R_i(\delta)$ with decreasing γ_i . Experimental data on $R_i(\alpha)$ ¹⁵, is plotted as shaded regions in the left panel of Fig.3. Performing the χ^2 analysis between the ImQMD predictions and the experimental data on $R_i(\alpha)$, the range of the symmetry potential parameter $0.45 \leq \gamma_i \leq 1.0$ are obtained within 2σ . Furthermore, the ImQMD predictions on the $R(X = \delta)$ (lines) as a function of rapidity are calculated and shown in the middle panel of fig.3 as lines, the star symbols represent measured values of R_7 obtained from the yield ratios of 7Li and 7Be at $b = 6fm$ ¹⁷. It can be seen that the calculation of the shapes and magnitude of the rapidity dependence of the isospin transport ratios reproduces the trends accurately. The corresponding χ^2 analysis on R_7 with calculations at $b = 6$ and $7fm$ favors the region $0.45 \leq \gamma_i \leq 0.95$ within 2σ uncertainties.

In order to see the cluster effects on the isospin transport ratio R_i , a tracer defined by the isospin asymmetry of the heaviest fragments with $Z \geq 20$ in projectile region is adopted in the transport model simulation for peripheral HICs ($b = 6fm$). The right panel in fig.3 show the R_i calculated with $X = \delta(Z_{max} > 20)$ (open diamonds) and open circles represent the results from the $X = \delta$ near the projectile rapidity as previous discussed. Independent of the isospin tracer we adopted, R_i obtained with soft symmetry case ($\gamma_i = 0.5$) is smaller than those obtained with stiff symmetry potential case ($\gamma_i = 2.0$). Another side, the values of R_i obtained with the new tracer $X = \delta(Z_{max} > 20)$ are larger than that with $X = \delta$ constructed from emitted nucleons and fragments near the projectile rapidity. It is caused by the cluster emission effects and the dynamical properties of the isospin diffusions. In HICs process, the neutrons (protons) of the projectile or target mainly transfer to the lower density neck region and then break up into IMFs and nucleons, few

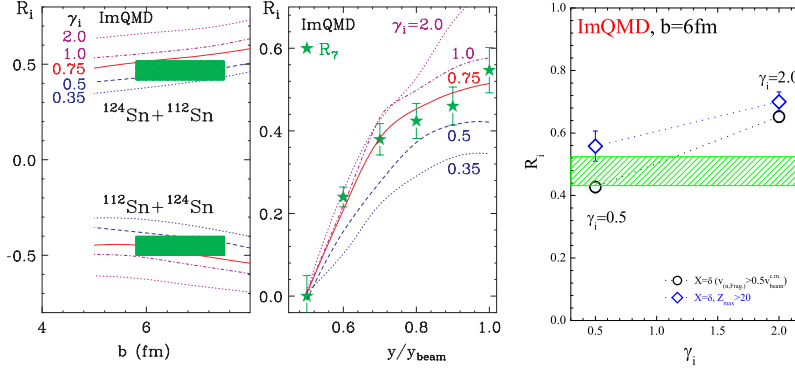
6 *Yingxun Zhang*


Fig. 3. Left panel: The calculated results on isospin transport ratios from the ImQMD model (lines) as a function of impact parameters for different values of γ_i and the experiment data $R_i(\alpha)$ (shaded regions). Middle panel: ImQMD calculations on the isospin transport ratios as a function of rapidity for different γ_i at $b = 6\text{ fm}$ and the experiment data on R_7 as a function of rapidity (star symbols)³⁶. Right panel: Isospin transport ratios obtained from different isospin tracer, $X = \delta(N, \text{Frag})$ (open circles) and $X = \delta(Z_{max} > 20)$ (open diamonds) in projectile region

nucleons from target residues diffuse to the projectile residues or vice versa due to the short diffusion time scale at $E/A = 50\text{ MeV}$. It leads the larger values of R_i for the new tracer $X = \delta(Z_{max} > 20)$. So, study the R_i with these different isospin tracer will help us to understand the dynamic effects on isospin diffusion in HICs and give a new constraint on the density dependence of symmetry energy.

3. Summary and outlook

In summary, the reaction mechanism of the central and peripheral collisions are investigated for $^{112,124}\text{Sn} + ^{112,124}\text{Sn}$ at $E/A = 50\text{ MeV}$ for different impact parameters. The results show that the reactions systems do not reach the global thermal equilibrium even for $\text{Sn} + \text{Sn}$ central collisions at $E/A = 50\text{ MeV}$ and the effects of cluster emission are important for both central and peripheral collisions. Three observables, double n/p ratios, isospin diffusion and the rapidity distribution the ratio R_7 are analyzed with the Improved Quantum Molecular Dynamics model. The results show that these three observables are sensitive to the density dependence of symmetry energy. By comparing calculation results to the data, the consistent constraints on the density dependence of symmetry energy can be obtained. Furthermore, the analysis of the coalescence-invariant $DR(n/p)$ ratio and the isospin transport ratios $R_i(X = \delta(Z_{max} > 20))$ show that the influence of the cluster emission on the double n/p ratios and the isospin transport ratio are important. However, the large uncertainties on the data implies that the improvements in the precision of data should be done in the near future, and accurate constraints on the density dependence of symmetry energy should be complemented from many

aspects, such as giant dipole resonances, pygmy dipole resonance, and mass data and some new observables from HICs and the observed properties of neutron star.

This work has been supported by the Chinese National Science Foundation under Grants 10675172, 10175093, 10235030 and the U.S. National Science Foundation under Grants PHY-0216783, 0456903, 060007, 0800026 and the High Performance Computing Center(HPCC) at Michigan State University.

References

1. Bao-An Li et al., *Phys. Rep.* **464** (2008) 113.
2. A.W. Steiner et al., *Phys. Rep.* **411** (2005) 325.
3. P. Danielewicz, *Nucl. Phys. A* **727** (2003) 233.
4. Pawel Danielewicz et al., *Nucl. Phys. A* **818** (2009) 36.
5. A.W. Steiner, *Phys. Rev. C* **77** (2008) 035805.
6. B. G. Todd-Rutel and J. Piekarewicz, *Phys. Rev. Lett* **95** (2005) 122501.
7. J. M. Lattimer and M. Prakash, *Science* **304** (2004) 536.
8. P. Danielewicz, R. Lacey, W.G. Lynch, *Science* **298** (2002) 1592.
9. C. Fuchs, *Prog. Part. Nucl. Phys* **56** (2006) 1.
10. D.H.Youngblood, H. L. Clark, and Y.-W. Lui, *Phys. Rev. Lett* **82**, (1999) 691
11. A. Brown, *Phys. Rev. Lett* **85** (2000) 5296
12. H.S. Xu, et al., *Phys. Rev. Lett.* **85** (2000) 716.
13. M.B. Tsang, et al., *Phys. Rev. Lett.* **86** (2001) 5023.
14. D.V. Shetty, et al., *Phys. Rev. C* **70** (2004) 011601.
15. M.B. Tsang, et al., *Phys. Rev. Lett* **92** (2004) 062701.
16. L.W.Chen, et al., *Phys. Rev. Lett* **94** (2005) 032701.
17. T. X. Liu et al., *Phys. Rev. C* **76**, (2007) 034603.
18. B.A.Li and L.W.Chen, *Phys. Rev. C* **72**, (2005)064611.
19. Yingxun Zhang, P.Danielewicz, M.Famiano, Zhuxia Li, W.G.Lynch, M.B.Tsang, *Phys. Lett B* **664** (2008) 145.
20. M.A. Famiano, T. Liu, W.G. Lynch, et al., *Phys. Rev. C* **97** (2006) 052701.
21. B.A. Li, C.M. Ko, Z. Ren, *Phys. Rev. Lett.* **78** (1997) 1644.
22. B.-A. Li, L.-W. Chen, G.-C. Yong, W. Zuo, *Phys. Lett B* **634** (2006) 378.
23. B.A. Li, *Phys. Rev. Lett.* **85** (2000) 4221; *Nucl. Phys. A* **734** (2004) 593c.
24. G.-C. Yong, B.-A. Li, L.-W. Chen, *Phys. Rev. C* **73** (2006) 034603.
25. W.Trautmann, et al., *arXiv/nucl-ex:0907.2822*.
26. Z.G.Xiao, B.A.Li, L.W.Chen, G.C.Yong, M.Zhang, *Phys. Rev. Lett.* **102** (2009) 062502.
27. Yingxun Zhang, Zhuxia Li, *Phys. Rev. C* **71** (2005) 024604.
28. Yingxun Zhang, Zhuxia Li, *Phys. Rev. C* **74** (2006) 014602.
29. J. Aichelin, A. Rosenhauer, G. Peilert, H. Stocker, W. Greiner, *Phys. Rev. Lett.* **58** (1987) 1926.
30. J. Cugnon, et al., *Nucl. Instrum. Methods Phys. Res. B* **111** (1996) 215.
31. R.Nebauer, J.Aichelin, et al., *Nucl. Phys. A* **658** (1999)67
32. A. S. Botvina et al., *Phys. Rev. C* **65**, 044610 (2002).
33. A. Ono et al., *Phys. Rev. C* **68**, 051601(R) (2003).
34. Yingxun Zhang, Zhuxia Li,P. Danielewicz, *Phys. Rev. C* **75** (2007) 034615.
35. L.Shi, P.Danielewicz, *Phys. Rev. C* **68** (2003)064604.
36. M.B.Tsang,Yingxun Zhang, P.Danielewicz, M.Famiano, Zhuxia Li, W.G.Lynch and A.W.Steiner, *Phys. Rev. Lett.* **102** (2009) 122701